

Invariance of quantum scattering rate coefficients to anisotropy of atom-molecule interactions

Xuyang Guo*

Department of Chemistry, University of British Columbia, Vancouver, B.C. V6T 1Z1, Canada

Kirk W. Madison

Department of Physics and Astronomy, University of British Columbia, Vancouver, B.C. V6T 1Z1, Canada

James L. Booth

Physics Department, British Columbia Institute of Technology, Burnaby, B.C. V5G 3H2, Canada

Roman V. Krems

*Department of Chemistry & Stewart Blusson Quantum Matter Institute,
University of British Columbia, Vancouver, B.C. V6T 1Z1, Canada*

(Dated: July 8, 2025)

Quantum scattering calculations for strongly interacting molecular systems are computationally demanding due to the large number of molecular states coupled by the anisotropy of atom - molecule interactions. We demonstrate that thermal rate coefficients for total (elastic + inelastic) atom - molecule scattering are insensitive to the interaction anisotropy of the underlying potential energy surface. In particular, we show that the rate coefficients for Rb-H₂ and Rb-N₂ scattering at room temperature can be computed to 1% accuracy with anisotropy set to zero, reducing the complexity of coupled channel quantum scattering calculations to numerical solutions of a single differential equation. Our numerical calculations and statistical analysis based on Gaussian process regression elucidate the origin and limitations of the invariance of the total scattering rate coefficients to changes in atom - molecule interaction anisotropy.

I. INTRODUCTION

Quantum scattering calculations of rate coefficients for molecular collisions are widely used for astrophysical models [1–5], as benchmarks of experimental measurements [6–10], and to elucidate mechanisms of energy transfer observed in molecular dynamics experiments [10–14]. Total (elastic + inelastic) scattering rate coefficients are essential inputs into methods using laser-cooled atoms to determine ambient gas density under high and ultra-high vacuum conditions via collision-induced heating and trap loss measurements [15–23]. For this sensor application, it is desired that the uncertainty of the rate coefficients is below 1% [17]. It is also desirable for these experiments to know the uncertainty of the computed collision rate coefficients. The uncertainty of the rate coefficients can be estimated by repeated quantum scattering calculations with underlying potential energy surfaces (PES) varied within their errors. However, quantum scattering calculations for strongly interacting molecular systems are computationally demanding due to the large number of molecular states coupled by the anisotropy of atom - molecule interactions. For example, rigorous quantum scattering calculations of room-temperature rate coefficients for Li-N₂ and Rb-N₂ collisions relevant for vacuum metrology require as many as 742 rotational states coupled by the interac-

tion anisotropy for convergence [24].

Recent work has investigated the probability distributions of cross sections for atom - molecule scattering that result from a distribution of interaction potential inputs to the calculations [25, 26]. Ref. [26] showed that reliable probabilistic predictions can be obtained with significantly reduced numerical effort. This result is relevant for the task of determining the uncertainty of a computed collision rate coefficient and demonstrates the feasibility of making predictions of experimentally relevant observables for certain systems previously considered out of reach of quantum dynamics theory. In other work motivated by vacuum metrology, it was found that certain, thermally averaged, atomic and molecular collision observables are invariant, or weakly sensitive, to changes of underlying interaction potentials at short inter-particle distances [17–19, 27]. Ref. [28] identified the range of parameters over which atom-atom collision rate coefficients exhibit this type of short-range invariance. Together, these results can be exploited to reduce the complexity of quantum scattering calculations without compromising their accuracy.

In the present work, we show that thermal rate coefficients for total atom - molecule scattering are invariant or weakly sensitive to changes in the interaction anisotropy. As a result, accurate rate coefficients for total scattering can be computed with single-channel quantum scattering calculations, using only the isotropic contribution of the atom - molecule interaction potential. We demonstrate that this invariance stems from thermal averaging, consistent with the results for quantum diffractive scat-

* Corresponding author: xyguo@chem.ubc.ca

tering in Refs. [17, 27, 28]. We perform a comprehensive analysis to examine the response of total thermal collision rate coefficients to the variations in both short-range and long-range parts of anisotropic potentials. This work is based on rigorous quantum scattering calculations employing the most accurate available interaction potentials for Rb-N₂ and Rb-H₂ collisions. We illustrate the invariance by treating the collision observables as probabilistic predictions determined by a distribution of interaction potentials [26, 28]. We show that the distributions of total rate coefficients are highly concentrated in changes of anisotropy, yielding consistent collision rate coefficients over a wide range of interaction potentials for Rb-H₂ and Rb-N₂ thermal collisions. We explore the boundaries of the invariance with respect to the strength of anisotropy of the interaction potentials. The observed boundaries significantly exceed typical uncertainties in anisotropic potentials from electronic structure calculations [24, 29]. Finally, we examine in detail the difference between multi-channel and single-channel calculations of total collision rate coefficients. We show that the difference is smaller than 1% of the rate coefficient magnitudes even for the atom-molecule collision systems with strong anisotropy and inelastic scattering.

II. METHOD

A. Scattering calculations

We calculate and analyze rate coefficients for collisions between trapped ⁸⁷Rb atoms and homonuclear molecules (²H₂ and ²⁸N₂) in a thermal background gas at temperature T . We treat the diatomic molecules as rigid rotors initially in a rotational state with a fixed value j of the rotational angular momentum. The rate coefficients $\kappa_j(T)$ are computed by integrating the cross sections $\sigma_j(\tilde{E})$ with the Maxwell-Boltzmann distribution

$$\kappa_j(T) = \sqrt{\frac{8k_B T}{\pi m}} \frac{1}{(k_B T)^2} \int_0^\infty E \sigma_j(\tilde{E}) \exp\left(-\frac{E}{k_B T}\right) dE, \quad (1)$$

where k_B is the Boltzmann constant, m is the mass of the molecule, E is the kinetic energy of the incident particle, $\tilde{E} = \mu E/m$ is the collision energy, and μ is the reduced mass of the collision complex.

We use rigorous close-coupling (CC) calculations to compute $\sigma_j(\tilde{E})$. The CC approach is well documented elsewhere [30–34]. Here, we present a brief description of the most relevant details. The collision cross sections $\sigma_j(\tilde{E})$ are obtained from the numerical solutions of the time-independent Schrödinger equation represented as a system of coupled differential equations

$$\left[\frac{d^2}{dR^2} - \frac{l'(l'+1)}{R^2} + k_{j'}^2 \right] F_{j'l'}^{Jj}(R) = \sum_{j''} \sum_{l''} U_{j''l'';j'l'}^J F_{j''l''}^{Jj}(R), \quad (2)$$

where R is the atom-molecule distance, l is the orbital angular momentum of the collision complex, j is the rotational angular momentum of the molecule, $J = j + l$ is the total angular momentum, and $U_{j''l'';j'l'}^J$ are determined by the matrix elements of the atom - molecule interaction potential described in the next section. The wave number $k_{j'}$ is defined as

$$k_{j'}^2 = \frac{2\mu}{\hbar^2} [E_{\text{total}} - B_r j'(j'+1)], \quad (3)$$

where B_r is the rotational constant of the diatomic molecule, and E_{total} is the total energy of the collision complex.

We use the log-derivative method [35] to integrate the coupled equations (2) and match the numerical solutions to the scattering boundary conditions, yielding the scattering matrix S , as described, for example, in Ref. [36, 37]. The state-resolved cross sections for the $j \rightarrow j'$ transitions in atom - molecule collisions are then computed as

$$\sigma_{jj'}(\tilde{E}) = \frac{4\pi}{(2j+1)k_j^2} \sum_{J=0}^{\infty} \sum_{l=|J-j|}^{J+j} \sum_{l'=|J-j'|}^{J+j'} (2J+1) \times |\delta_{jj'} \delta_{ll'} - S^J(jl; j'l')|^2, \quad (4)$$

where $j = j'$ and $j \neq j'$ corresponds to elastic and inelastic scattering, respectively. The cross section in Eq. (1) is computed as

$$\sigma_j(\tilde{E}) = \sum_{j'} \sigma_{jj'}(\tilde{E}) \quad (5)$$

We allow the maximum rotational angular momentum j_{max} to be 6 for ²H₂ and 26 for ²⁸N₂. This ensures convergence of cross sections at the highest collision energy considered to within $\leq 0.1\%$. We include enough terms in the partial wave sum (4) to ensure convergence of cross sections to $\leq 0.1\%$ and extend the range of incident particle energy in Eq. (1) to ensure convergence of the thermal rate coefficients to $\leq 0.25\%$. The number of partial waves required for convergence depends on the reduced mass of the collision complex and the collision energy \tilde{E} . We include quantum states with $l \leq 200$ for Rb-H₂ collisions and ≤ 650 for Rb-N₂ collisions.

For further analysis, we also calculate the rate coefficients $\kappa_j(T)$ assuming the partial cross sections are determined solely by elastic scattering from the purely isotropic, long-range part of the interaction potential. The corresponding scattering phase shifts obtained from the semi-classical Jeffreys-Born approximation [27]:

$$\eta_l(k) = \frac{3\pi}{16} \left(\frac{\mu C_6}{\hbar^2} \right) \frac{k^4}{(l + \frac{1}{2})^5} + \frac{5\pi}{32} \left(\frac{\mu C_8}{\hbar^2} \right) \frac{k^6}{(l + \frac{1}{2})^7} + \frac{35\pi}{256} \left(\frac{\mu C_{10}}{\hbar^2} \right) \frac{k^8}{(l + \frac{1}{2})^9}, \quad (6)$$

where C_n are the coefficients in the isotropic, long-range expansion of the interaction potential:

$$\lim_{R \rightarrow \infty} V(R) = -\frac{C_6}{R^6} - \frac{C_8}{R^8} - \frac{C_{10}}{R^{10}}. \quad (7)$$

The cross-section in Eq. 4 can then be simplified to:

$$\sigma(\tilde{E}) = \frac{4\pi}{k^2} \sum_{l=0}^{\infty} (2l+1) \sin^2 \eta_l. \quad (8)$$

The resulting rate coefficients are determined solely by the elastic long-range part of interaction potentials.

B. Atom-molecule interaction potential

Within the rigid rotor approximation for the diatomic molecule, the atom - molecule interaction potential is a function of two coordinates. We use the Jacobi coordinates (R, θ) defined as the magnitude R of vector \mathbf{R} joining the centers of mass of the atom and the diatomic molecule and the angle θ between the axis of the diatomic molecule and \mathbf{R} . The atom-molecule interaction potential $V(R, \theta)$ is represented as a sum of Legendre polynomials

$$V(R, \theta) = \sum_{\lambda=0}^{\infty} V_{\lambda}(R) P_{\lambda}(\cos \theta). \quad (9)$$

For homonuclear diatomic molecules, the expansion contains only terms with even values of λ . The expansion coefficients $V_{\lambda}(R)$ are computed using the global PES from Ref. [38] for Rb-H₂ and Ref. [24] for Rb-N₂. We include terms with $\lambda = 0, 2, 4$, and 6 in Eq. (9) for both interaction potentials considered here.

The leading expansion coefficient V_0 characterizes the isotropic part of the interaction potential, which predominantly determines elastic scattering. The expansion coefficients V_{λ} with $\lambda > 0$ describe the anisotropy of the atom - molecule interaction that leads to inelastic scattering.

This work aims to investigate the response of the thermal collision rate coefficients [Eq. (1)] to the variations in the isotropic and anisotropic parts of the interaction potentials at short range R . To accomplish this, we model $V_{\lambda}(R)$ using Morse long-range (MLR) functions [39]

$$V_{\lambda}(R) = D_{e,\lambda} \mathcal{F}_{\lambda}(R), \quad (10)$$

where

$$\mathcal{F}_{\lambda}(R) = \left(1 - \frac{u_{\text{LR}}(R)}{u_{\text{LR}}(R_{e,\lambda})} \exp[-\beta(R) \cdot y_p^{\text{eq}}(R)] \right)^2, \quad (11)$$

$D_{e,\lambda}$ is the well depth, $R_{e,\lambda}$ is the equilibrium distance of the corresponding expansion coefficient. The function $\beta(R)$ is defined as a polynomial function

$$\beta(R) = y_p^{\text{ref}} \beta_{\infty} + [1 - y_p^{\text{ref}}] \sum_{i=0}^N \beta_i [y_q^{\text{ref}}]^i \quad (12)$$

of the radial variables, or reduced coordinates $y_{p,q}^{\text{ref}}(R)$

$$y_{p,q}^{\text{ref}}(R) = \frac{R^{p,q} - R_{\text{ref}}^{p,q}}{R^{p,q} + R_{\text{ref}}^{p,q}} \quad (13)$$

where R_{ref} is the reference distance [40]. The integer powers p and q are fixed to 4 and 5, respectively, following Ref. [39]. The radial variable y_p^{eq} takes the form of Eq. (12) with $R_{\text{ref}} = R_e$. The constraint parameter β_{∞} is fixed to $\ln\{2D_e/u_{\text{LR}}(R_e)\}$. The long-range potential u_{LR} in Eq. (10) has the asymptotic form

$$u_{\text{LR}}(R) = D_6 \frac{C_6}{R^6} + D_8 \frac{C_8}{R^8} + D_{10} \frac{C_{10}}{R^{10}}, \quad (14)$$

where D_n is the damping function defined as the generalized Douketis function [41, 42]

$$D_n(r, s) = \left(1 - \exp \left(-\frac{b(s)(\rho R)}{n} - \frac{c(s)(\rho R)^2}{n^{1/2}} \right) \right)^{n+s}, \quad (15)$$

where $b(s)$ and $c(s)$ are system-independent parameters determined by the choice of s . In this work, we choose $s = -1$, $b = 3.3$, and $c = 0.423$, following Ref. [39]. The dimensionless parameter $\rho = \frac{2\rho_M \rho_{\text{BG}}}{(\rho_M + \rho_{\text{BG}})}$ [41] is calculated as the harmonic mean of the atomic counterparts $\rho_i = \left(\frac{\text{IP}_i}{\text{IP}_H} \right)^{\frac{2}{3}}$, where IP_i and IP_H represent the ionization potentials of the respective molecule and atomic hydrogen. We fit the expansion coefficients of the *ab initio* potentials in Ref. [24] and [38] by the non-linear least squares method to obtain the MLR parameters. Compared to the *ab initio* energies, the root mean squared error of the resulting fits is smaller than 1 cm⁻¹.

C. Statistical analysis

In addition to rigorous CC calculations, we adopt a statistical analysis approach to examine the response of total collision rate coefficients to variations in both the short-range part and long-range part of the interaction anisotropy as well as changes in the magnitude of the rotational constant of the diatomic molecule. We begin by treating the equilibrium distance $R_{e,\lambda=2}$, the well depth magnitude $D_{e,\lambda=2}$ and the long-range interaction coefficient $C_{6,\lambda=2}$ as variables with wide ranges of values, leading to a distribution of interaction potentials of varying anisotropy. To ensure the generality of conclusions, we also vary $D_{e,\lambda=0}$ and the rotational constant B_r of the molecule. The rate coefficients κ_{tot} are thus considered to be functions of five variables.

To obtain the global dependence of κ_{tot} on these five variables, we build a Gaussian process (GP) regression model of κ_{tot} trained by rigorous multi-channel scattering calculations at randomly sampled combinations of $R_{e,\lambda=2}$, $D_{e,\lambda=2}$, $C_{6,\lambda=2}$, $D_{e,\lambda=0}$, and B_r . GP regression is a supervised learning algorithm that uses a set of

N input-output pairs $\mathcal{D} = \{(\mathbf{x}_i, y_i)\}_{i=1}^N$ to infer a target function $y(\mathbf{x})$. In the present work, $\kappa_{\text{tot}} \Rightarrow y$ and $(R_{e,\lambda=2}, D_{e,\lambda=2}, C_{6,\lambda=2}, D_{e,\lambda=0}, B_r) \Rightarrow \mathbf{x} \in \mathbb{R}^5$. Once trained, a GP model can be used to predict the value of y at an arbitrary point \mathbf{x}_* of input space as follows[43]:

$$y(\mathbf{x}_*) = \mathbf{k}^\top(\mathbf{x}_*)(\mathbf{K} + \sigma_n^2 \mathbf{I})^{-1} \mathbf{y}, \quad (16)$$

where \mathbf{y} is a vector collecting N training points y_i , \mathbf{k} is the vector of size N with elements given by the values of a kernel function $k(\mathbf{x}_i, \mathbf{x}_*)$ and \mathbf{K} is the $N \times N$ matrix with elements given by the values of the kernel function $k(\mathbf{x}_i, \mathbf{x}_j)$ for $\mathbf{x}_i, \mathbf{x}_j \in \mathcal{D}$. The value of σ_n^2 is set to zero because the training points y_i are the results of the CC calculations, which produce noiseless data. The kernel

function is chosen to be

$$\begin{aligned} k(\mathbf{x}_i, \mathbf{x}_j) = & A_1^2 \left(1 + \frac{\sqrt{3}r}{\ell_1}\right) \exp\left(-\frac{\sqrt{3}r}{\ell_1}\right) \\ & + A_2^2 \left(1 + \frac{\sqrt{5}r}{\ell_2} + \frac{5r^2}{3\ell_2^2}\right) \exp\left(-\frac{\sqrt{5}r}{\ell_2}\right) \\ & + A_3^2 \exp\left(-\frac{r^2}{2\ell_3^2}\right) + A_4^2 \left(1 + \frac{r^2}{2\alpha\ell_4^2}\right)^{-\alpha} \\ & + A_5^2 (\mathbf{x}_i^\top \mathbf{x}_j) \end{aligned} \quad (17)$$

where $r = \|\mathbf{x}_i - \mathbf{x}_j\|$ denotes the Euclidean distance between the input data points, ℓ_i are the characteristic length-scale parameters, α is the shape parameter of the rational quadratic (RQ) kernel, and A_i are the amplitudes of different components of the kernel function. The parameters of the kernel function are estimated by type-II maximum likelihood estimation [43]. The accuracy of the resulting GP models is illustrated in Fig. 1. Fig. 1 includes rate coefficients from the entire range of the input parameters and shows the error of the GP model predictions as the departure from the diagonal broken line. The models illustrated in Fig. 1 are trained by 3300 (upper panel) and 1500 (lower panel) CC calculations of κ_{tot} and produce a maximum error of 2.5 % over randomly sampled test sets including 1900 (upper panel) and 3700 (lower panel) values of calculated κ_{tot} . We consider the following ranges of the input variables: $R_{e,\lambda=2} \in [0.25, 7] \text{ \AA}$, $D_{e,\lambda=2} \in [1, 110] \text{ cm}^{-1}$, $C_{6,\lambda=2} \in [0.5, 350] E_h \cdot a_0^6$, $D_{e,\lambda=0} \in [1, 110] \text{ cm}^{-1}$, $B_r \in [0, 10] \text{ cm}^{-1}$.

Given the GP model of the rate coefficients $\kappa_{\text{tot}} = f(R_{e,\lambda=2}, D_{e,\lambda=2}, C_{6,\lambda=2}, D_{e,\lambda=0}, B_r)$, we treat a subset of the variables as random variables in order to examine the dependence of κ_{tot} on the remaining variables. We consider GP model predictions marginalized over the random variables as well as predictions for multiple, fixed samples of the random variables. Marginalization refers to integrating the predictive distribution from the GP model over the distribution of the random variables, thereby incorporating the variation in those variables into the analysis of the dependence of κ_{tot} on the remaining variables. This allows for a comprehensive analysis of the dependence of κ_{tot} on the interaction anisotropy, accounting for the effects of variations in the strength of the isotropic part of the interaction potential and the rotational constant of the molecule on the resulting conclusions. The GP models are used to supplement direct multi-channel scattering calculations with specific subsets of the variables considered here. In these calculations, the remaining variables are kept fixed, which corresponds to examining cuts in the five-dimensional dependence of κ_{tot} on the interaction potential parameters and the rotational constant.

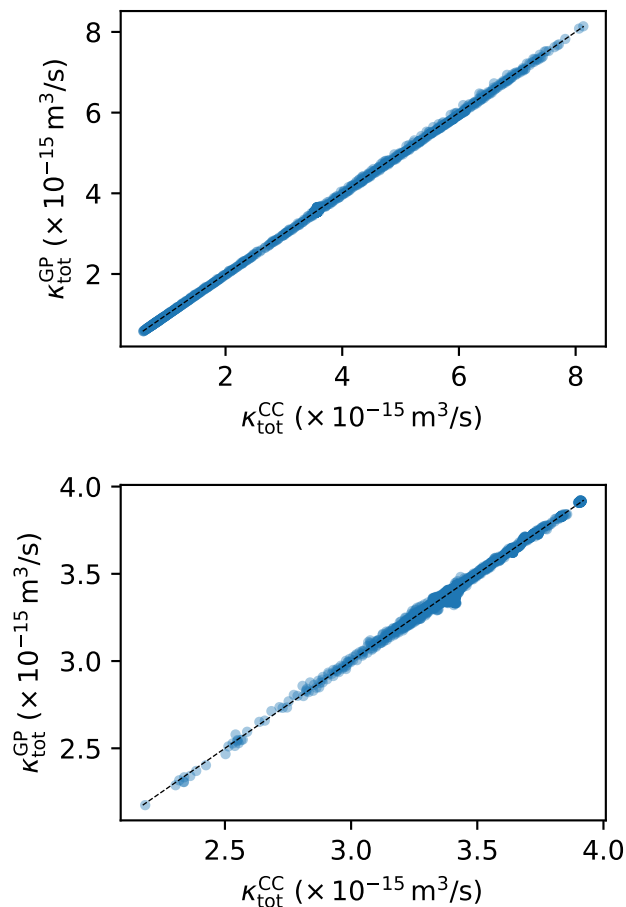


FIG. 1. Comparison of κ_{tot} predicted by the 5D GP model with the results of CC calculations. The CC calculations for training and testing the GP models are performed with the reduced mass, $C_{6,\lambda=0}$ and $R_{e,\lambda=0}$ corresponding to the Rb-H₂ (upper) and Rb-N₂ (lower) collision systems.

TABLE I. Rate coefficients (in units of 10^{-15} m³/s) for elastic (κ_{el}), inelastic (κ_{inel}) and total (κ_{tot}) scattering of Rb with H₂ and N₂ initially in the rotational state j . The temperature is $T = 294.15$ K. The results for κ_{el} , κ_{inel} , and κ_{tot} are from cross sections computed with converged CC calculations and full PESs. The results for κ_{single} are from the single-channel differential equation with the corresponding isotropic part of the full PES obtained by setting all $V_{\lambda>0}(R)$ in Eq. (9) to zero. The results for κ_{SC} are computed using the semi-classical Jeffreys-Born approximation 6 with the long-range expansion coefficients for $V_{\lambda=0}(R \rightarrow \infty)$.

| j | System | κ_{el} | κ_{inel} | κ_{tot} | κ_{single} | κ_{SC} |
|-----|-------------------|----------------------|------------------------|-----------------------|--------------------------|----------------------|
| 0 | Rb-H ₂ | 3.575 | 0.0003 | 3.576 | 3.567 | 5.964 |
| | Rb-N ₂ | 3.107 | 0.306 | 3.413 | 3.395 | 3.467 |
| 2 | Rb-H ₂ | 3.577 | 0.0004 | 3.578 | 3.567 | — |
| | Rb-N ₂ | 3.287 | 0.109 | 3.396 | 3.395 | — |
| 4 | Rb-H ₂ | 3.577 | 0.0001 | 3.577 | 3.567 | — |
| | Rb-N ₂ | 3.341 | 0.058 | 3.399 | 3.395 | — |
| 6 | Rb-H ₂ | 3.577 | 0.00001 | 3.577 | 3.567 | — |
| | Rb-N ₂ | 3.370 | 0.057 | 3.427 | 3.395 | — |

III. RESULTS

We begin by calculating rate coefficients for total Rb-H₂(j) and Rb-N₂(j) scattering at room temperature using three methods: (i) rigorous multi-channel CC calculations with the best fits of full PES described in Section II A; (ii) single-channel scattering calculations using only the isotropic part $V_{\lambda=0}(R)$ of the interaction poten-

tials; (iii) semi-classical Jeffreys-Born approximation (6) based on the long-range part of $V_{\lambda=0}(R \rightarrow \infty)$. The results are presented in Table I for molecules initially in different rotational states $j = 0, 2, 4, 6$.

We note a very good agreement between κ_{tot} from full CC calculations and κ_{SC} based on the semi-classical Jeffreys-Born approximation for Rb-N₂ collisions but not for Rb-H₂ collisions. This illustrates that quantum scattering of Rb by N₂ is qualitatively different from Rb-H₂ collisions, as a consequence of the dramatic difference in the corresponding PES and reduced masses. In the present work, we use the PES for Rb-N₂ and Rb-H₂ collision complexes as a starting point for our analysis and perform calculations with the reduced mass for Rb-N₂ and Rb-H₂ collisions.

We observe a remarkable agreement between κ_{tot} from full CC calculations and κ_{single} from single-channel calculations for both Rb-N₂ and Rb-H₂ collisions and for all rotational states of the molecule considered. The results for κ_{single} are obtained from the cross sections computed by integrating the single-channel differential equation that corresponds to Eq. (2) with all $V_{\lambda>0}(R)$ in Eq. (9) set to zero. Thus, the PES used for the computation of κ_{single} ignores entirely the anisotropy of the atom - molecule interaction. The agreement between κ_{tot} and κ_{single} is particularly interesting for Rb-N₂ collisions and for collisions of molecules in excited states, which exhibit significant rates of inelastic scattering. In the following sections, we examine in detail the response of thermal rate coefficients to variations in the interaction anisotropy in order to elucidate the extent and generality of the agreement between the results of multi-channel and

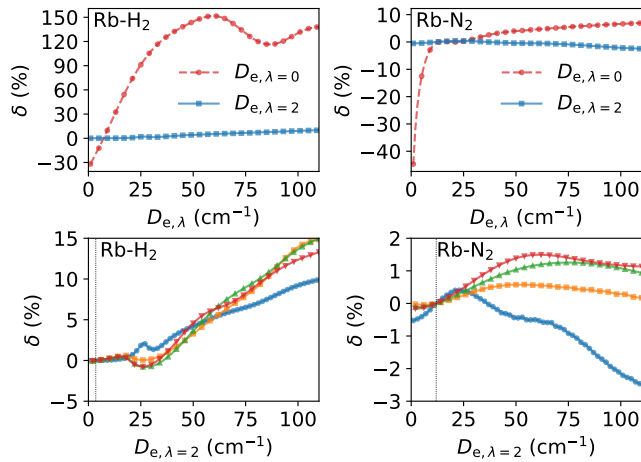


FIG. 2. CC calculations of the relative deviation (17) for collisions of Rb with H₂ (left) and N₂ (right). Upper panels: Relative deviation (18) for collisions of molecules in the ground rotational state as functions of the well depth magnitude for the isotropic $V_{\lambda=0}$ (circles) and leading anisotropic $V_{\lambda=2}$ (squares) Legendre expansion coefficients of the full PES. Lower panels: The relative deviation (18) as functions of $D_{e,\lambda=2}$ for collisions of molecules in the rotational states $j = 0$ (circles), $j = 2$ (squares), $j = 4$ (triangles), $j = 6$ (inverted triangles).

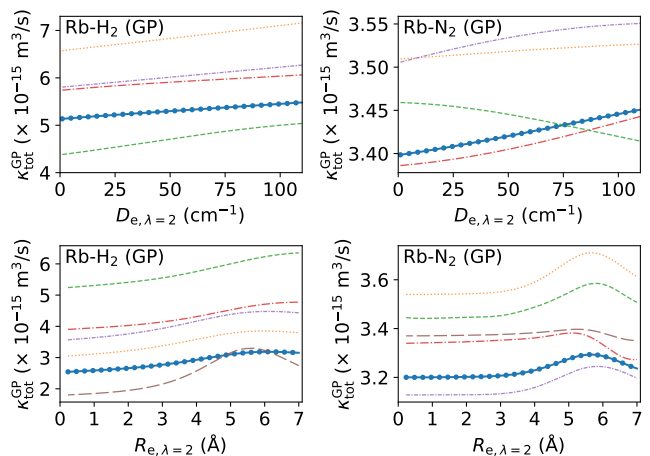


FIG. 3. Rate coefficients κ_{tot} from the GP models as functions of $D_{e,\lambda=2}$ (upper panels) and $R_{e,\lambda=2}$ (lower panels). The GP models are trained by the CC calculations performed with the reduced mass, $C_{6,\lambda=0}$ and $R_{e,\lambda=0}$ corresponding to the Rb-H₂ (left) and Rb-N₂ (right) collision systems. The lines with the symbols represent κ_{tot} marginalized over the variables not shown on the x -axis. The solid lines show samples of $\kappa_{\text{tot}} = f(R_{e,\lambda=2}, D_{e,\lambda=2}, C_{6,\lambda=2}, D_{e,\lambda=0}, B_r)$ for random combinations of the variables not shown on the x -axis.

single-channel quantum scattering calculations of κ_{tot} .

A. Invariance to short-range anisotropy

To analyze the effect of anisotropy, we first compute the dependence of the total collision rate coefficients on $D_{e,\lambda=0}$ and $D_{e,\lambda=2}$ using direct CC calculations as described in Section II A. We vary either $D_{e,\lambda=0}$ or $D_{e,\lambda=2}$ to compute the deviation of the resulting rate coefficient κ'_{tot} from the corresponding value in Table I. Figure 2 (top panels) illustrates the relative deviation

$$\delta = \frac{\kappa'_{\text{tot}} - \kappa_{\text{tot}}}{\kappa_{\text{tot}}} \times 100\% \quad (18)$$

as a function of either $D_{e,\lambda=0}$ or $D_{e,\lambda=2}$ for Rb-H₂ ($j = 0$) and Rb-N₂ ($j = 0$) collisions. For these calculations, when $D_{e,\lambda=0}$ or $D_{e,\lambda=2}$ is varied, all other parameters of PES and the molecular constants are fixed to the values corresponding to the specific collision system under examination.

The results show that κ_{tot} are sensitive to changes in $D_{e,\lambda=0}$ but remain nearly constant over a wide range of $D_{e,\lambda=2}$. More specifically, the relative changes δ remain within 10% for Rb-H₂ ($j = 0$) collision and 3% for Rb-N₂ ($j = 0$) collision, across the wide range of $D_{e,\lambda=2}$ from 1 to 110 cm⁻¹. It is instructive to examine the response of total scattering to variation of $D_{e,\lambda=2}$ for molecules in excited rotational states, which permit both excitation and relaxation inelastic transitions. We repeat the calculations of the total rate coefficients for molecules initially in the $j = 2, 4$, and 6 rotational states. The resulting values of δ are shown in Fig. 2 (lower panels) for a wide range of $D_{e,\lambda=2}$. For reference, the values of $D_{e,\lambda=2}$

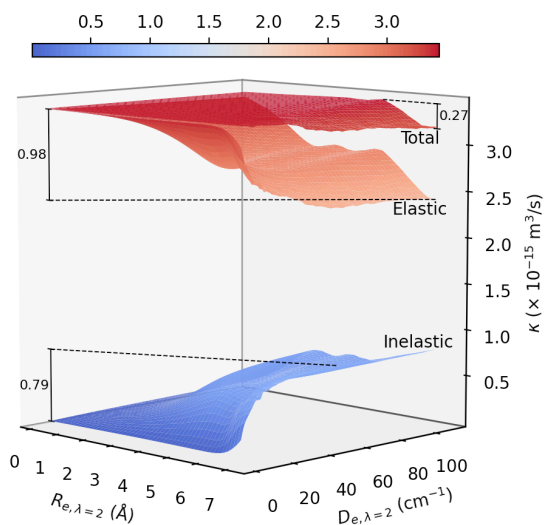


FIG. 4. Rate coefficients for total, elastic, and inelastic scattering of Rb with N₂ ($j = 0$) as functions of $R_{e,\lambda=2}$ and $D_{e,\lambda=2}$ from CC calculations.

corresponding to the best fits of the corresponding PES are shown in Fig. 2 by the vertical dotted lines.

To illustrate the lack of sensitivity to $D_{e,\lambda=2}$ for a wide range of molecular collision parameters, we analyze the distribution of κ_{tot} as a function of $D_{e,\lambda=2}$ obtained by random sampling from the 5D GP model described in Section II C and by marginalization of the GP model predictions over $R_{e,\lambda=2}$, $C_{6,\lambda=2}$, $D_{e,\lambda=0}$ and B_{r} . The upper panels of Fig. 3 illustrate that the distributions exhibit a significant variance with the randomly sampled parameters, but are squeezed in $D_{e,\lambda=2}$. The lower panels of Fig. 3 illustrate the dependence of κ_{tot} on the position of the minimum $R_{e,\lambda=2}$. It can be seen that a very big change in $R_{e,\lambda=2}$ (corresponding to a very big change in the interaction anisotropy) is required to induce a change of κ_{tot} exceeding 1%. We note that these distributions reflect the dependence of κ_{tot} on $D_{e,\lambda=2}$ for a range of molecules with different rotational constants and a distribution of PES with widely different anisotropies as determined by both $R_{e,\lambda=2}$ and $D_{e,\lambda=2}$.

While κ_{tot} appears to be invariant to changes in short-range anisotropy, the rate coefficients for elastic and inelastic scattering change significantly with the interaction anisotropy. This is illustrated in Fig. 4 that depicts κ_{el} , κ_{inel} and κ_{tot} for Rb - N₂ ($j = 0$) collisions obtained with direct CC calculations as functions of $R_{e,\lambda=2}$ and $D_{e,\lambda=2}$. Figure 4 shows that the elastic rate coefficients decrease as the inelastic rate coefficients grow, restricting

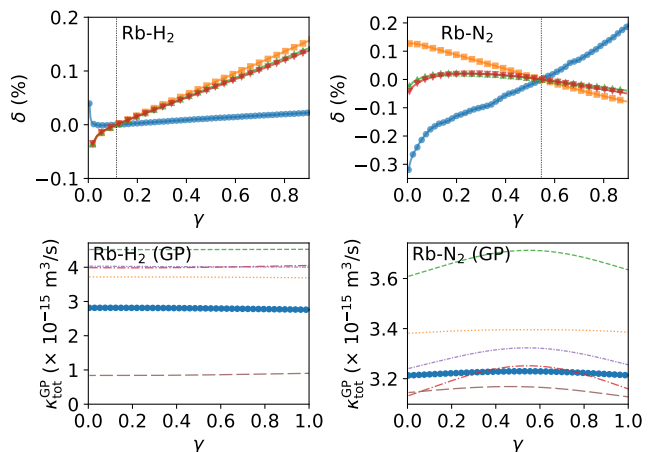


FIG. 5. Upper panels: The relative deviation (18) as a function of $\gamma = C_{6,\lambda=2}/C_{6,\lambda=0}$ for collisions of Rb with H₂ (left) and N₂ (right) initially in the rotational state $j = 0$ (circles), $j = 2$ (squares), $j = 4$ (triangles), $j = 6$ (inverted triangles). Lower panels: Rate coefficients κ_{tot} from the GP models as functions of γ . The lines with the symbols represent κ_{tot} marginalized over $R_{e,\lambda=2}$, $D_{e,\lambda=2}$, $D_{e,\lambda=0}$ and B_{r} . The solid lines show samples of $\kappa_{\text{tot}} = f(R_{e,\lambda=2}, D_{e,\lambda=2}, C_{6,\lambda=2}, D_{e,\lambda=0}, B_{\text{r}})$ for random combinations of $R_{e,\lambda=2}$, $D_{e,\lambda=2}$, $D_{e,\lambda=0}$ and B_{r} . The GP models are trained by the CC calculations performed with the reduced mass, $C_{6,\lambda=0}$ and $R_{e,\lambda=0}$ corresponding to the Rb-H₂ (left) and Rb-N₂ (right) collision systems.

the variation of κ_{tot} despite the wide range of $R_{e,\lambda=2}$ and $D_{e,\lambda=2}$ considered. We note that the PES corresponding to the values of $R_{e,\lambda=2}$ and $D_{e,\lambda=2}$ from the opposite limits of the corresponding ranges are qualitatively different. Thus, PES with small values of $D_{e,\lambda=2}$ exhibit one minimum in the T-shaped configuration (defined as $\theta = 90$ degrees), whereas large values of $D_{e,\lambda=2}$ introduce an additional minimum at the linear atom - molecule ($\theta = 0$ degrees) geometry.

Table II quantifies the variation of κ_{tot} with the change of both the isotropic part and the anisotropy of PES at short range. To obtain the results in Table II, we vary the equilibrium distance R_e for both the isotropic $\lambda = 0$ and anisotropic $\lambda = 2$ contributions to the interaction potential. This results in a distribution of κ_{tot} . We compute the distribution of κ_{tot} by sampling from a wide range of PES parameters $R_{e,\lambda} \in [0.25, 7]$ Å and $D_{e,\lambda} \in [1, 110]$ cm⁻¹ and the distribution of κ_{tot} by sampling from the range of $R_{e,\lambda}$ and $D_{e,\lambda}$ encompassing ± 10 % deviations from the values in the MLR (10) fits of the most accurate fits of the *ab initio* potentials for Rb-H₂ and Rb-N₂. The first sampling is designed to explore the response to κ_{tot} to extreme changes of PES. The second sampling is designed to vary the PES within a range closer to an expected error of quantum chemistry calculations. We note that the ± 10 % variation of the PES parameters, though considered here as small, significantly exceeds the estimated uncertainties of the *ab initio* calculations and the fits of the interaction potentials [24, 39].

B. Invariance to long-range anisotropy

In this section, we examine the response of the total thermal rate coefficients to the anisotropy of PES at long range, quantified by the parameter $\gamma = C_{6,\lambda=2}/C_{6,\lambda=0}$, where $C_{6,\lambda=0}$ and $C_{6,\lambda=2}$ are the leading coefficients in expansion (7) of $V_{\lambda=0}$ and $V_{\lambda=2}$, respectively. We fix $C_{6,\lambda=0}$ to the values of the best fit of the corresponding *ab initio* potentials and generate a series of PES in the range of γ from 0 to 1 by varying $C_{6,\lambda=2}$. The upper panels of

TABLE II. Relative standard deviation (in %) of the distributions of κ_{tot} for total Rb + M collisions corresponding to the variation of $R_{e,\lambda} \in [0.25, 7]$ Å and $D_{e,\lambda} \in [1, 110]$ cm⁻¹ (wide range) and within the $\pm 10\%$ range defined as $R_{e,\lambda} \in [0.9 \times R_{e,\lambda=0}, 1.1 \times R_{e,\lambda=0}]$ and $D_e \in [0.9 \times D_{e,\lambda=0}, 1.1 \times D_{e,\lambda=0}]$, where $R_{e,\lambda=0}$ and $D_{e,\lambda=0}$ are the well depth and the equilibrium distance from the MLR fits (10) of the corresponding *ab initio* potentials.

| M | Variable parameters | Wide range | $\pm 10\%$ |
|----------------|------------------------------------|------------|------------|
| H ₂ | $D_{e,\lambda=2}, R_{e,\lambda=2}$ | 3.4 | 0.004 |
| H ₂ | $D_{e,\lambda=0}, R_{e,\lambda=0}$ | 57.9 | 10.2 |
| N ₂ | $D_{e,\lambda=2}, R_{e,\lambda=2}$ | 1.4 | 0.08 |
| N ₂ | $D_{e,\lambda=0}, R_{e,\lambda=0}$ | 5.9 | 1.5 |

Fig. 5 show the departure of κ_{tot} from the corresponding values in Table I as functions of γ for collisions of Rb with H₂ and N₂ in different rotational states. The results show that the long-range anisotropy, even when $C_{6,\lambda=2} = C_{6,\lambda=0}$ does not alter κ_{tot} by more than a small fraction of one percent.

The lower panels of Fig. 5 show the dependence of κ_{tot} on γ predicted by the GP model described in Section II C. The lines with the symbols show the predictions marginalized over $R_{e,\lambda=2}, D_{e,\lambda=2}, D_{e,\lambda=0}$ and B_r , whereas the solid lines show model predictions for random samples from various combinations of $R_{e,\lambda=2}, D_{e,\lambda=2}, D_{e,\lambda=0}$ and B_r . It is clear from these results that κ_{tot} remains invariant to changes in γ for a wide range of PES with different anisotropies and a wide range of rotational constants of the diatomic molecule.

C. Single-channel vs multi-channel scattering calculations

The numerical complexity of multi-channel scattering calculations scales as $O(N^3)$ where N is the number of coupled channels. Converged scattering calculations for the total thermal rate coefficients for Rb-N₂ collisions at room temperature require $N = 742$ coupled channels. Based on the results in Sections III A and III B, we argue that single-channel ($N = 1$) quantum scattering calculations using only the isotropic part $V_{\lambda=0}(R)$ of PES can achieve similar accuracy for total thermal rate coefficients as multi-channel CC calculations.

To further support this argument and show that this conclusion extends to a wide range of molecular systems, we express the atom-molecule interaction potentials as

$$V(R, \theta) = V_0 \left(1 + \sum_{\lambda=2,4,6} \frac{D_{e,\lambda}}{D_{e,\lambda=0}} \cdot \frac{\mathcal{F}_\lambda(R)}{\mathcal{F}_0(R)} P_\lambda(\cos \theta) \right), \quad (19)$$

where $\mathcal{F}_\lambda(R)$ is the radial term in Eq. (11). The term with $\lambda = 2$ is scaled by the ratio $D_{e,\lambda=2}/D_{e,\lambda=0}$. We vary $D_{e,\lambda=2}$ from 1 to 110 cm⁻¹ and set $D_{e,\lambda=0}$ to 20, 50, 100 cm⁻¹. We then perform both converged multi-channel calculations with full PES and single-channel calculations using only $V_{\lambda=0}$ to compute the total scattering rate coefficients. The relative difference of the single- and multi-channel results is quantified by \mathcal{D} , defined as

$$\mathcal{D} = \frac{\kappa_{\text{single}} - \kappa_{\text{CC}}}{\kappa_{\text{CC}}} \times 100\%, \quad (20)$$

where κ_{single} and κ_{CC} are the total rate coefficients from the single- and multi-channel CC scattering calculations, respectively. The relative difference is presented in the upper panel of Fig. 8. The results show that the largest differences for $D_{e,\lambda=0} = 20, 50, 100$ cm⁻¹ are -0.88%, 0.37%, and -0.089%, despite the inelastic rate contributions reaching up to 19%, 18%, and 22% of the total

rate coefficients as shown in the lower panel of Fig. 8. The results suggest that single-channel calculations can yield total rate coefficients with the same accuracy as multi-channel calculations for atom-molecule collisions with strong interaction anisotropy.

We further illustrate the agreement between single- and multi-channel calculations for molecules with different rotational constants B_r . We consider a range of the rotational constant from 0 to 10 cm^{-1} . For reference, the magnitude of the rotational constant for N_2 is 1.998 cm^{-1} [44, 45]. We use the GP model of the rate coefficients for $\text{Rb-N}_2(j=0)$ collisions to examine the dependence of κ_{tot} on $D_{e,\lambda=2}$. Fig. 7 shows the model predictions marginalized over the remaining three variables ($R_{e,\lambda=2}$, $C_{6,\lambda=2}$ and $D_{e,\lambda=0}$). This accounts for a wide range of PES corresponding to different values of $D_{e,\lambda=0}$ and long-range interaction parameters. The results show that the change of the magnitude of κ_{tot} remains under 1 % for all rotational constants considered despite the variation of $D_{e,\lambda=2}$ over a wide range from 0 to 100 cm^{-1} . We also observe a very weak dependence of κ_{tot} on the rotational constant of the molecule.

We conjecture that the agreement between the total rate coefficients from single-channel scattering calcula-

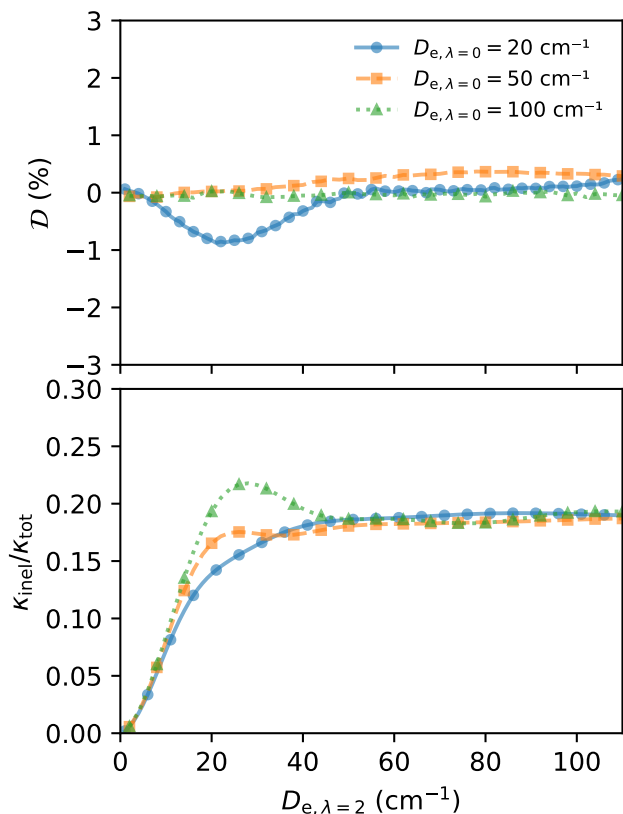


FIG. 6. Relative deviations (18) and relative contribution of inelastic scattering to the total scattering rate coefficient as functions of $D_{e,\lambda=2}$ for collisions of Rb with $\text{N}_2(j=0)$ for $D_{e,\lambda=0} = 20$ (circles), 50 (squares) and 100 cm^{-1} (triangles).

tions with $V_{\lambda=0}$ and multi-channel CC calculations is a consequence of the Maxwell-Boltzmann averaging (1) that diminishes the effect of the glory oscillations and reduces the sensitivity of quantum diffractive scattering to PES at short range so long as the collision velocities do not exceed a certain threshold [27, 28, 46–48]. To illustrate the effect of thermal averaging, we compute the cross sections as functions of the collision energy for scattering of Rb by molecules with different rotational constants. The results of the single-channel and multi-channel CC calculations are shown in the upper panel of Fig. 8. The energy dependences of the cross sections from the single-channel calculation and the results of the CC calculations for different rotational constants oscillate about the same background value. Thermal averaging of the three different energy dependences yields the rate coefficients within 0.16 %.

This remarkable agreement of the thermally averaged rate coefficients occurs despite drastically different dynamics of atom - molecule collisions for molecules with different rotational constants, as illustrated in Fig. 8. The upper right panel of Fig. 8 shows the energy dependences of the elastic and inelastic cross sections for molecules with $B_r = 0.09$ and $B_r = 0 \text{ cm}^{-1}$. We observe that the amplitude of the glory oscillations decreases with decreasing B_r , as a result of the enhancement of inelastic scattering. The lower panels of Fig. 8 further show the elastic and inelastic scattering cross sections at a fixed collision energy $E = k_B T = 204.44 \text{ cm}^{-1}$ as functions of the total angular momentum J . We observe that, for low values of J , the elastic scattering cross sections decrease and the inelastic scattering cross sections increase with decreasing B_r . The total scattering cross sections

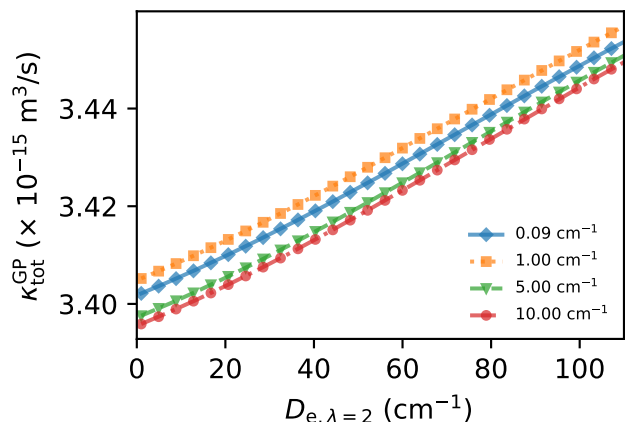


FIG. 7. Rate coefficients κ_{tot} from the 5D GP model as functions of $D_{e,\lambda=2}$, for the collision systems with rotational constant $B_r = 0.09$ (blue diamonds), 1.0 (orange squares), 5 (green triangles), and 10 cm^{-1} (red circles). The CC calculations for training and testing the GP model are performed with the reduced mass, $C_{6,\lambda=0}$ and $R_{e,\lambda=0}$ corresponding to the Rb-N_2 collision system. Lines with symbols represent κ_{tot} marginalized over all variables except B_r and $D_{e,\lambda=2}$.

for large J are universal for collisions of molecules with different rotational constants, consistent with the observation in Ref. [17]. The glory oscillations, which are due to the interference between partial waves in elastic scattering channels [27, 46–48], vanish as inelastic scattering gains magnitude. At the same time, the results in Fig. 8 show that the increase in inelastic cross sections with decreasing B_r compensates for the decrease in elastic cross sections, consistent with the observation in Fig. 4.

IV. SUMMARY

We have presented a comprehensive analysis of the response of thermally averaged total rate coefficients for atom-molecule collisions to variations in both short-range and long-range anisotropy of the atom - molecule PES. We use rigorous quantum scattering theory, the interaction potentials based on high-level electronic structure calculations for Rb–N₂ and Rb–H₂ collisions, and the statistical analysis approach based on Gaussian process regression to examine in detail the extent and the origin of the invariance of total collision rate coefficients to changes in the interaction anisotropy.

It is illustrated that the invariance of the total scattering rate coefficients to the interaction anisotropy is independent of the initial rotational state and the rotational constant of the diatomic molecule. To explore the limits of the invariance with respect to the strength of the interaction anisotropy, we examine the response of the total rate coefficients to the wide variations of PES. Our calculations illustrate that the total scattering rate coefficients change by less than 1 % as $D_{e,\lambda=2}$ is increased by a factor of 10 and the long-range anisotropy parameter $\gamma = C_{6,\lambda=0}/C_{6,\lambda=2}$ is increased by a factor of 20 from the values corresponding to the best fits of PES for Rb–N₂ and Rb–H₂ collisions. We note that these ranges are much wider than typical uncertainties from electronic structure calculations [24, 39].

The invariance of total scattering to the interaction anisotropy suggests that thermal collision rates for total atom-molecule scattering can be computed using only the isotropic part of PES, which requires the integration of a single (uncoupled) differential equation instead of a large number of coupled equations for scattering calculations with full PES. Our analysis shows that single-channel scattering calculations agree with full CC calculations of total scattering rate coefficients for Rb–N₂ ($j = 0, 2, 4, 6$) and Rb–H₂ ($j = 0, 2, 4, 6$) collisions to within 0.92%. This agreement remains within 0.88% for molecules with a wide range of rotational constants, despite the inelastic rate contributions reaching up to 29% of the total collision rate coefficients.

Our scattering calculations systematically illustrate that the invariance of total scattering rate coefficients is due to the mutual compensation of elastic and inelastic scattering rate coefficients. The agreement between the results of single- and multi-channel scattering calcu-

lations is shown to be due to the Maxwell-Boltzmann averaging 1. Thermal averaging also reduces the dependence of the total scattering rate coefficients on the rotational constant of the molecule. We have shown that the glory oscillations in the scattering cross sections for molecules with small rotational constants are significantly suppressed by the enhancement of inelastic scattering. While the glory oscillations remain significant for molecules with large rotational constants, thermal averaging reduces the influence of the glory oscillations, consistent with the observations in Refs. [27, 28, 46–48].

ACKNOWLEDGMENTS

We acknowledge the financial support from the Natural Sciences and Engineering Research Council of Canada (NSERC grants RGPIN-2019-04200, RGPAS-2019-00055) and the Canadian Foundation for Innovation (CFI project 35724). This work was conducted at the Center for Research on Ultra-Cold Systems (CRUCS) and was supported in part by computational resources and services provided by Advanced Research Computing at the University of British Columbia. X.G., K.W.M. and R.V.K. acknowledge support from the Deutsche Forschungsgemeinschaft within the RTG 2717 program.

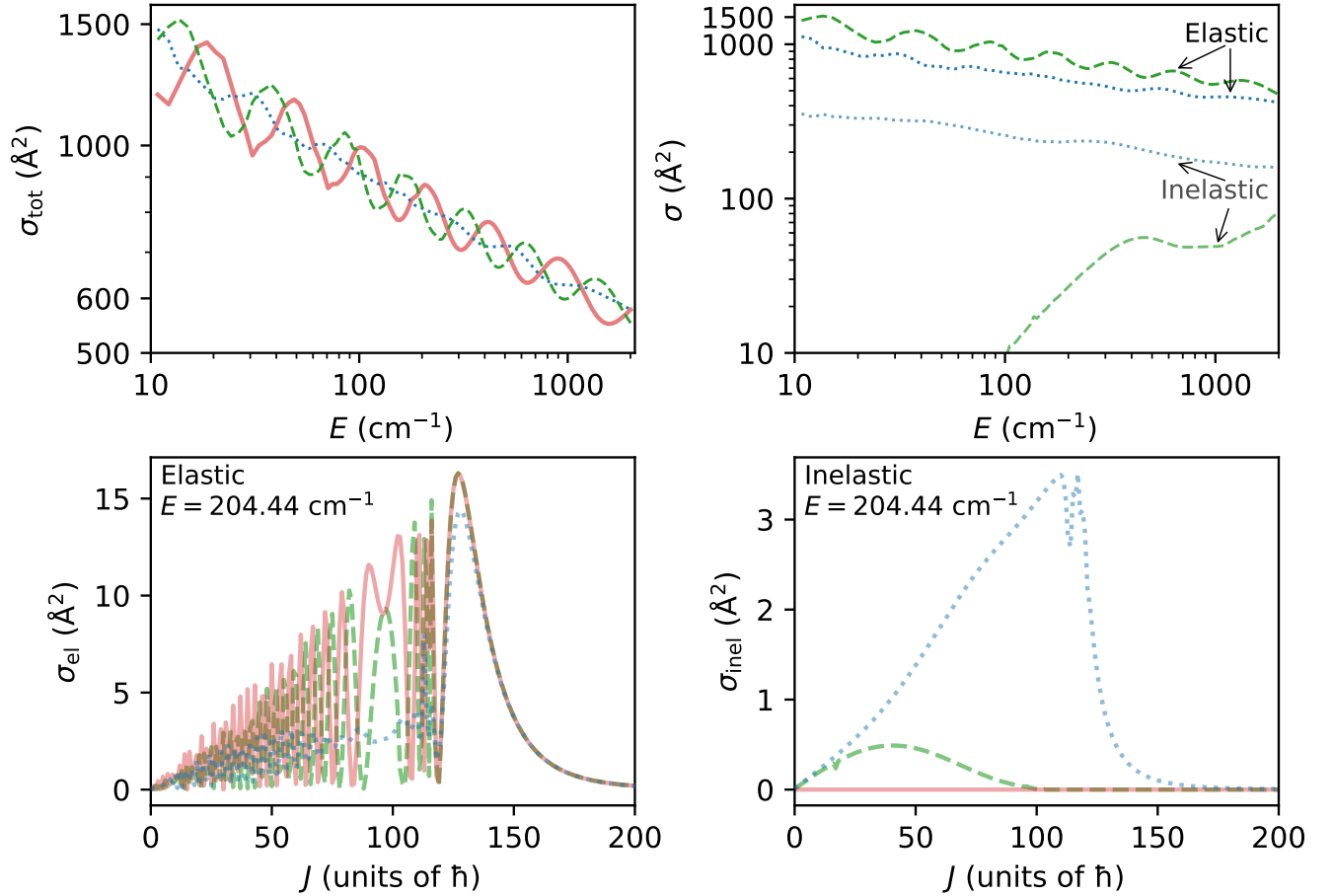


FIG. 8. Cross sections from CC calculations performed with the reduced mass, $C_{6,\lambda=0}$ and $R_{e,\lambda=0}$ corresponding to the Rb-N₂ collision system with the rotational constant B_r varied to 0.09 (blue dots) and 10 cm⁻¹ (green dashes), and from single-channel calculations (red solid curves). The $D_{e,\lambda=0}$ and $D_{e,\lambda=2}$ are varied to 100 cm⁻¹. Upper panels: Total (left), elastic (right), and inelastic (right) cross sections as functions of collision energy E . Lower panels: Elastic (left) and inelastic (right) cross sections as functions of total angular momentum J with the collision energy $E = 204.44$ cm⁻¹.

-
- [1] A. Faure, Collisional rate coefficients for astrophysics, Proc. Int. Astron. Union **18**, 123–132 (2022).
- [2] C. Boursier, B. Mandal, D. Babikov, and M. L. Dubernet, New H₂O-H₂O collisional rate coefficients for cometary applications, Mon. Not. R. Astron. Soc. **498**, 5489 (2020).
- [3] Hernández, M. I., Tejada, G., Fernández, J. M., and Montero, S., Rate coefficients for H₂:H₂ inelastic collisions in the ground vibrational state from 10 to 1000 k, Astron. Astrophys. **647**, A155 (2021).
- [4] Mandal, Bikramaditya and Babikov, Dmitri, Rate coefficients for rotational state-to-state transitions in H₂O + H₂O collisions for cometary and planetary applications, as predicted by mixed quantum-classical theory, Astron. Astrophys. **671**, A51 (2023).
- [5] L. González-Sánchez, A. Veselinova, A. Martín Santa Daría, E. Yurtsever, R. Biswas, K. Giri, N. Sathya-murthy, U. Lourderaj, R. Wester, and F. A. Gianturco, Computed rotational collision rate coefficients for recently detected anionic cyanopolyynes, Astrophys. J. **960**, 40 (2023).
- [6] H. Son, J. J. Park, W. Ketterle, and A. O. Jamison, Collisional cooling of ultracold molecules, Nature **580**, 197 (2020).
- [7] L. Wiesenfeld, Quantum nature of molecular vibrational quenching: Water-molecular hydrogen collisions, J. Chem. Phys. **155**, 071104 (2021).
- [8] Y. Liu, M.-G. Hu, M. A. Nichols, D. Yang, D. Xie, H. Guo, and K.-K. Ni, Precision test of statistical dynamics with state-to-state ultracold chemistry, Nature **593**, 379 (2021).
- [9] Q. Hong, M. Bartolomei, C. Coletti, A. Lombardi, Q. Sun, and F. Pirani, Vibrational energy transfer in CO+N₂ collisions: A database for V-V and V-T/R quantum-classical rate coefficients, Molecules **26** (2021).
- [10] P. Paliwal, N. Deb, D. M. Reich, A. v. d. Avoird, C. P. Koch, and E. Narevicius, Determining the nature of quantum resonances by probing elastic and reactive scattering in cold collisions, Nat. Chem. **13**, 94 (2021).

- [11] Qct calculations of $O_2 + O$ collisions: Comparison to molecular beam experiments, *J. Chem. Phys.* **153** (2020).
- [12] M. Besemer, G. Tang, Z. Gao, A. van der Avoird, G. C. Groenenboom, S. Y. van de Meerakker, and T. Karman, Glory scattering in deeply inelastic molecular collisions, *Nat. Chem.* **14**, 664 (2022).
- [13] N. Mukherjee, Quantum-controlled collisions of H_2 molecules, *J. Phys. Chem. A* **127**, 418 (2023).
- [14] B. Mandal, C. Joy, D. Bostan, A. Eng, and D. Babikov, Adiabatic trajectory approximation: a new general method in the toolbox of mixed quantum/classical theory for collisional energy transfer, *J. Phys. Chem. Lett.* **14**, 817 (2023).
- [15] K. W. Madison, A cold atom based UHV pressure standard, Personal Communication (2012).
- [16] J. L. Booth, D. E. Fagnan, B. G. Klappauf, K. W. Madison, and J. Wang, Method and device for accurately measuring flux density, U.S. Patent No. 8,803,072 B2 (2014).
- [17] J. L. Booth, P. Shen, R. V. Krems, and K. W. Madison, Universality of quantum diffractive collisions and the quantum pressure standard, *New J. Phys.* **21**, 102001 (2019).
- [18] P. Shen, K. W. Madison, and J. L. Booth, Realization of a universal quantum pressure standard, *Metrologia* **57**, 025015 (2020).
- [19] P. Shen, K. W. Madison, and J. L. Booth, Refining the cold atom pressure standard, *Metrologia* **58**, 022101 (2021).
- [20] D. S. Barker, J. A. Fedchak, J. Klos, J. Scherschligt, A. A. Sheikh, E. Tiesinga, and S. P. Eckel, Accurate measurement of the loss rate of cold atoms due to background gas collisions for the quantum-based cold atom vacuum standard, *AVS Quantum Sci.* **5**, 035001 (2023).
- [21] P. Shen, E. Frieling, K. R. Herperger, D. Uhland, R. A. Stewart, A. Deshmukh, R. V. Krems, J. L. Booth, and K. W. Madison, Cross-calibration of atomic pressure sensors and deviation from quantum diffractive collision universality for light particles, *New J. Phys.* **25**, 053018 (2023).
- [22] R. A. Stewart, P. Shen, J. L. Booth, and K. W. Madison, Measurement of Rb-Rb van der Waals coefficient via quantum diffractive universality, *Phys. Rev. A* **106**, 052812 (2022).
- [23] E. Frieling, R. A. Stewart, J. L. Booth, and K. W. Madison, Cross-calibration of quantum atomic sensors for pressure metrology, *AVS Quantum Sci.* **6**, 024404 (2024).
- [24] J. Klos and E. Tiesinga, Elastic and glancing-angle rate coefficients for heating of ultracold Li and Rb atoms by collisions with room-temperature noble gases, H_2 , and N_2 , *J. Chem. Phys.* **158**, 014308 (2023).
- [25] J. Cui and R. V. Krems, Elastic and inelastic collisions of $^2\Sigma$ molecules in a magnetic field, *Phys. Rev. A* **88**, 042705 (2013).
- [26] M. Morita, R. V. Krems, and T. V. Tscherbul, Universal Probability Distributions of Scattering Observables in Ultracold Molecular Collisions, *Phys. Rev. Lett.* **123**, 013401 (2019).
- [27] J. L. Booth and K. W. Madison, Revising the universality hypothesis for room-temperature collisions, *Phys. Rev. A* **110**, 052802 (2024).
- [28] X. Guo, K. W. Madison, J. L. Booth, and R. V. Krems, Boundaries of universality of thermal collisions for atom-atom scattering, *Phys. Rev. A* **110**, 063317 (2024).
- [29] A. Derevianko, S. G. Porsev, and J. F. Babb, Electric dipole polarizabilities at imaginary frequencies for hydrogen, the alkali-metal, alkaline-earth, and noble gas atoms, *At. Data Nucl. Data Tables* **96**, 323 (2010).
- [30] A. Arthurs and A. Dalgarno, The theory of scattering by a rigid rotator, *Proc. R. Soc. Lond. A* **256**, 540 (1960).
- [31] W. A. Lester, Calculation of cross sections for rotational excitation of diatomic molecules by heavy particle impact: Solution of the close-coupled equations, in *Atomic and Molecular Scattering*, Methods in Computational Physics: Advances in Research and Applications, Vol. 10, edited by B. Alder, S. Fernbach, and M. Rotenberg (Elsevier, 1971) pp. 211–241.
- [32] M. H. Alexander, Quantum study of the redistribution of flux during inelastic collisions, *J. Chem. Phys.* **95**, 8931 (1991).
- [33] D. E. Manolopoulos and M. H. Alexander, Quantum flux redistribution during molecular photodissociation, *J. Chem. Phys.* **97**, 2527 (1992).
- [34] R. B. Bernstein and B. Bederson, Atom—molecule collision theory: A guide for the experimentalist, *Phys. Today* **33**, 79 (1980).
- [35] D. E. Manolopoulos, An improved log derivative method for inelastic scattering, *J. Chem. Phys.* **85**, 6425 (1986).
- [36] B. Johnson, The multichannel log-derivative method for scattering calculations, *J. Comput. Phys.* **13**, 445 (1973).
- [37] D. Manolopoulos and R. Wyatt, Quantum scattering via the log derivative version of the kohn variational principle, *Chem. Phys. Lett.* **152**, 23 (1988).
- [38] S. Upadhyay, U. Dargyte, R. P. Prater, V. D. Dergachev, S. A. Varganov, T. V. Tscherbul, D. Patterson, and J. D. Weinstein, Enhanced spin coherence of rubidium atoms in solid parahydrogen, *Phys. Rev. B* **100**, 024106 (2019).
- [39] A. A. Medvedev, V. V. Meshkov, A. V. Stolyarov, and M. C. Heaven, *Ab initio* interatomic potentials and transport properties of alkali metal (M = Rb and Cs)—rare gas (Rg = He, Ne, Ar, Kr, and Xe) media, *Phys. Chem. Chem. Phys.* **20**, 25974 (2018).
- [40] R. J. Le Roy, N. S. Dattani, J. A. Coxon, A. J. Ross, P. Crozet, and C. Linton, Accurate analytic potentials for $Li_2(X^1\Sigma_g^+)$ and $Li_2(A^1\Sigma_u^+)$ from 2 to 90 Å, and the radiative lifetime of $Li(2p)$, *J. Chem. Phys.* **131**, 204309 (2009).
- [41] C. Douketis, G. Scoles, S. Marchetti, M. Zen, and A. J. Thakkar, Intermolecular forces via hybrid Hartree–Fock–SCF plus damped dispersion (HFD) energy calculations. An improved spherical model, *J. Chem. Phys.* **76**, 3057 (1982).
- [42] R. J. Le Roy, C. C. Haugen, J. Tao, and H. Li, Long-range damping functions improve the short-range behaviour of ‘MLR’ potential energy functions, *Mol. Phys.* **109**, 435 (2011).
- [43] C. Rasmussen and C. Williams, *Gaussian Processes for Machine Learning*, Adaptive Computation and Machine Learning series (MIT Press, 2005).
- [44] J. Bendtsen, The rotational and rotation-vibrational raman spectra of $^{14}N_2$, $^{14}N^{15}N$, and $^{15}N_2$, *J. Raman Spectrosc.* **2**, 133 (1974).
- [45] A. Lofthus and P. H. Krupenie, The spectrum of molecular nitrogen, *J. Phys. Chem. Ref. Data* **6**, 113 (1977).
- [46] R. B. Bernstein, Extrema in Velocity Dependence of Total Elastic Cross Sections for Atomic Beam Scattering: Relation to Di-atom Bound States, *J. Chem. Phys.* **37**, 1880 (1962).

- [47] R. B. Bernstein, Semiclassical Analysis of the Extrema in the Velocity Dependence of Total Elastic-Scattering Cross Sections: Relation to the Bound States, *J. Chem. Phys.* **38**, 2599 (1963).
- [48] M. Child, *Molecular Collision Theory*, Dover Books on Chemistry Series (Dover Publications, 1996).